

Efficient Non-parametric Bayesian Hawkes Processes

Rui Zhang^{1,2}¹ The Australian National UniversityChristian Walder^{1,2}Marian-Andrei Rizoiu^{1,2}Lexing Xie^{1,2}² Data 61, CSIRO, Australia

Abstract

In this paper, we develop a non-parametric Bayesian estimation of Hawkes process kernel functions. Our method is based on the cluster representation of Hawkes processes. We sample random branching structures, and thus split the Hawkes process into clusters of Poisson processes, where the intensity function of each of these processes is the non-parametric triggering kernel of the Hawkes process. We derive both a block Gibbs sampler and a *maximum a posteriori* estimator based on stochastic expectation maximization. On synthetic data, we show our method to be flexible and scalable, and on two large-scale Twitter diffusion datasets, we show our method to outperform the parametric Hawkes model. We observe that the learned non-parametric kernel reflects the longevity of different content types. Code has been made publicly available¹

1 Introduction

The Hawkes process (Hawkes, 1971) is a useful model to describe self-exciting point data in which every point increases the likelihood of arrival of new points. More specifically, every point causes the conditional intensity function $\lambda(\cdot)$ which modulates the arrival rate of new points to increase. An alternative understanding of the Hawkes process is the Poisson cluster process (Hawkes and Oakes, 1974) which categorizes points into *immigrants* and *offspring*. Immigrant points are generated independently at a rate of $\mu(\cdot)$ and offspring points are triggered by existing points at a rate of $\phi(\cdot)$. Points are structured into clusters, associated with each immigrant point, which is called the branching structure (an example shown in Fig. 1).

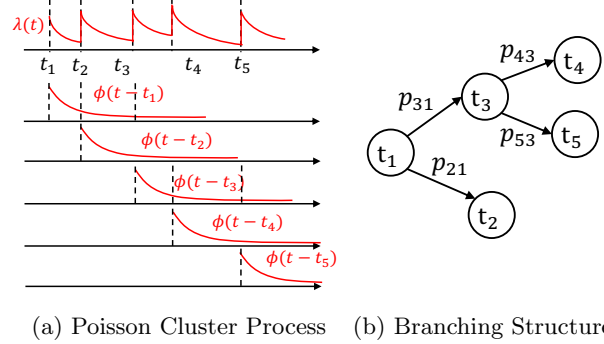


Figure 1: Cluster Representation of the Hawkes Process. (a) A Hawkes process with decaying triggering kernel $\phi(\cdot)$ has intensity $\lambda(t)$ which increases after each new point is generated. It can be represented as a cluster of Poisson processes $PP(\phi(t - t_i))$ associated with each t_i . For the triggering relationships shown in (a), a branching structure can be represented as (b), where $t_1 \rightarrow t_3$ represents t_1 triggers t_3 and p_{31} is the probability of t_3 being generated by t_1 .

Background & Motivations The Hawkes process has been applied to a wide range of problems. Mishra et al. (2016) employ the branching factor of the Hawkes process to predict popularity of tweets; Kurashima et al. (2018) predict human actions by the Hawkes process; information reliability and information source trustworthiness of online knowledge repositories are evaluated by the Hawkes process (Tabibian et al., 2017). Here, we address two difficulties of leveraging Hawkes processes in such applications: (1) the aforementioned work employ manually designed parametric Hawkes models which may not generalize well and (2) in particular cases, the shape of the Hawkes kernel might not be easy to deduce in advance.

A typical solution is the non-parametric estimation of the intensity function (Lewis and Mohler, 2011; Zhou et al., 2013; Eichler et al., 2017; Bacry et al., 2012; Bacry and Muzy, 2014; Kirchner, 2017). However, these are all frequentist methods, which do not allow to quantify the uncertainty of the learned kernels. There exist several work (Blundell et al., 2012; Rasmussen,

¹<https://github.com/RuiZhang2016/Efficient-Nonparametric-Bayesian-Hawkes-Processes>

2013; Rousseau et al., 2018) on the Bayesian inference for the Hawkes process. The main difficulty in developing a non-parametric Bayesian method is the quadratic time taken to compute the log-likelihood of the Hawkes process. The related work closest to this paper is the method of Rousseau et al. (2018), who employ Markov chain Monte Carlo (MCMC) to estimate the posterior of the Hawkes model. The main difference between this approach and ours is that our work uses the stochastic branching structure to accelerate the estimation of the posterior Hawkes process.

Contributions In this paper, we propose a general framework for the efficient non-parametric Bayesian inference of Hawkes processes. We exploit block Gibbs sampling (Ishwaran and James, 2001) to iteratively sample the latent branching structure, the background intensity $\mu(\cdot)$ and the triggering kernel $\phi(\cdot)$. In each iteration, the point data are decomposed as a cluster of Poisson processes based on the sampled branching structure. This is exemplified in Fig. 1, in which a Hawkes process (the top temporal axis) is decomposed into several Poisson processes (the following temporal axis), and the branching structure is inferred. Posterior $\mu(\cdot)$ and $\phi(\cdot)$ are estimated from the resulting clustered processes. Our framework is close to the stochastic Expectation-Maximization (EM) algorithm (Celeux and Diebolt, 1985) where posterior $\mu(\cdot)$ and $\phi(\cdot)$ are estimated in the M-step and random samples of $\mu(\cdot)$ and $\phi(\cdot)$ are drawn (Adams et al., 2009; Lloyd et al., 2015; Samo and Roberts, 2015; Walder and Bishop, 2017; Gugushvili et al., 2018). We adapt the approach of the recent non-parametric Bayesian estimation for Poisson process intensities, termed Laplace Bayesian Poisson process (LBPP) (Walder and Bishop, 2017), to estimate the posterior $\phi(\cdot)$ given the sampled branching structure. Furthermore, we explore the connection with the EM algorithm (Dempster et al., 1977) and develop a variant of our method as an approximate EM algorithm. On synthetic data, we show our method can infer the exponential and the cosine triggering kernels, and the fitting time of our method is linear to the number of points. On two large social media datasets, our method outperforms the parametric Hawkes process by as much as 22% in holdout log-likelihood.

2 Preliminaries

In this section, we introduce prerequisites: the Hawkes process and LBPP.

2.1 Hawkes Process

As introduced in Section 1, the Hawkes process can be specified by the conditional intensity function $\lambda(\cdot)$ which modulates the arrival rate of points. Mathematically, conditioned on a set of points $\{t_i\}_{i=1}^N$, the intensity $\lambda(\cdot)$ is expressed as (Hawkes, 1971)

$$\lambda(t) = \mu(t) + \sum_{t_i < t} \phi(t - t_i), \quad (1)$$

where $\mu(\cdot) : \mathbb{R} \rightarrow [0, \infty)$ and $\phi(\cdot) : \mathbb{R} \rightarrow [0, \infty)$ are the background intensity and the triggering kernel. The log-likelihood of $\{t_i\}_{i=1}^N$ given the background intensity $\mu(\cdot)$ and the triggering kernel $\phi(\cdot)$ is (Rubin, 1972)

$$\log p(\{t_i\}_{i=1}^N | \mu(\cdot), \phi(\cdot)) = \sum_{i=1}^N \log \left[\mu(t_i) + \sum_{t_j < t_i} \phi(t_i - t_j) \right] - \int_{\Omega} \mu(t) + \sum_{t_i < t} \phi(t - t_i) \, dm(t), \quad (2)$$

where Ω is the sampling domain of $\{t_i\}_{i=1}^N$ with measure m .

2.2 LBPP

LBPP (Walder and Bishop, 2017) has been proposed for the non-parametric Bayesian estimating the intensity of a Poisson process. To satisfy non-negativity of the intensity function, LBPP models a point process intensity $\lambda(\cdot)$ as a permanent process (Shirai and Takahashi, 2003), i.e., $\lambda = g \circ f$ where the link function $g(z) = \frac{1}{2}z^2$ and $f(\cdot)$ is Gaussian process (GP) distributed. Alternative link functions for non-negative intensities include $\exp(\cdot)$ (Rathbun and Cressie, 1994; Møller et al., 1998; Illian et al., 2012; Diggle et al., 2013) and $g(z) = \lambda^*(1 + \exp(-z))^{-1}$ (Adams et al., 2009) where λ^* is constant. The choice $g(z) = \frac{1}{2}z^2$ has analytical and computational advantages (Lloyd et al., 2016; Flaxman et al., 2017; Walder and Bishop, 2017; Lloyd et al., 2015) which lead to a linear time algorithm for LBPP.

LBPP exploits the Mercer expansion (Mercer, 1909) of the GP covariance function $k(x, y) \equiv \text{Cov}(f(x), f(y))$,

$$k(x, y) = \sum_{i=1}^K \lambda_i e_i(x) e_i(y), \quad (3)$$

where for LBPP the eigenfunctions $\{e_i(\cdot)\}_i$ are chosen to be orthonormal in $L^2(\Omega, m)$ for some sample space Ω with measure m . $f(\cdot)$ can be represented as a linear combination of $e_i(\cdot)$ (Rasmussen and Williams, 2005),

$$f(\cdot) = \omega^T \nu(\cdot), \quad (4)$$

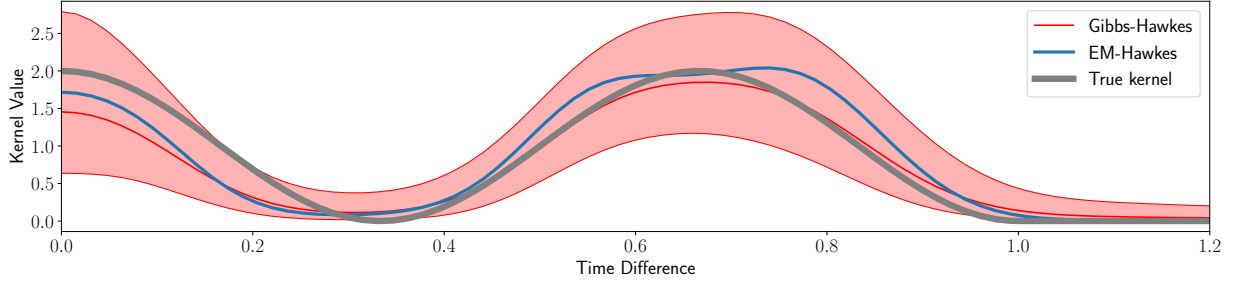


Figure 2: Triggering kernels estimated by the Gibbs-Hawkes method (Section 3) and the EM-Hawkes method (Section 4). The true kernel is plotted as the bold gray curve. We plot the median (red) and [0.1, 0.9] interval (filled red) of the approximate predictive distribution, along with the triggering kernel inferred by the EM Hawkes method (blue). The hyper-parameters a and b of the Gaussian process kernel (Eq. (17)) are set to 0.002.

and ω has a Gaussian prior, i.e., $\omega \sim \mathcal{N}(0, \Lambda)$ where $\Lambda = \text{diag}(\lambda_1, \lambda_2, \dots, \lambda_K)$ is a diagonal covariance matrix and $\nu(\cdot) = [e_1(\cdot), \dots, e_K(\cdot)]$ is a vector of basis functions. The posterior intensity at some t , $\lambda(t)$, requires estimating the posterior ω which is approximated by a normal distribution (a.k.a Laplace approximation) (Rasmussen and Williams, 2005):

$$\log p(\omega|X, \Omega, k) \approx \log \mathcal{N}(\omega|\hat{\omega}, Q), \quad (5)$$

where $X = \{t_i\}_{i=1}^N$ is a set of point data, Ω the sampling space and k the Gaussian process kernel function. $\hat{\omega}$ is selected as the mode of the true posterior and Q the negative inverse Hessian of the true posterior at $\hat{\omega}$:

$$\hat{\omega} = \underset{\omega}{\operatorname{argmax}} \log p(\omega|X, \Omega, k) \quad (6)$$

$$Q^{-1} = -\frac{\partial^2}{\partial \omega \partial \omega^T} \log p(\omega|X, \Omega, k) \Big|_{\omega=\hat{\omega}}. \quad (7)$$

The approximate posterior distribution of $f(t)$ is a normal distribution (Rasmussen and Williams, 2005):

$$f(t) \sim \mathcal{N}(\hat{\omega}^T \nu(t), \nu(t)^T Q \nu(t)) \equiv \mathcal{N}(\mu, \sigma^2). \quad (8)$$

Furthermore, the posterior distribution of $\lambda(t)$ is a Gamma distribution (Walder and Bishop, 2017):

$$\text{Gamma}(x|\alpha, \beta) \equiv \frac{\beta^\alpha x^{\alpha-1} e^{-\beta x}}{\Gamma(\alpha)}, \quad (9)$$

where

$$\alpha = \frac{(\mu^2 + \sigma^2)^2}{2\sigma^2(2\mu^2 + \sigma^2)} \quad \text{and} \quad \beta = \frac{\mu^2 + \sigma^2}{2\mu^2\sigma^2 + \sigma^4}.$$

3 Inference via Sampling

We now detail our efficient non-parametric Bayesian estimation algorithm, which samples the posterior of μ (constant background intensity) and $\phi(\cdot)$ (the triggering kernel). Our method starts with random $\mu_0, \phi_0(\cdot)$ and iterates by cycling through the following four steps (k is the iteration index):

- i Calculate $p(B|X, \phi_{k-1}, \mu)$, the distribution of the branching structure given the data, triggering kernel, and background intensity (see Section 3.1).
- ii Sample a B_k using $p(B|X, \phi_{k-1}, \mu)$ (see Section 3.1).
- iii Estimate $p(\phi|B_k, X)$ (Section 3.3) and $p(\mu|B_k, X)$ (Section 3.2).
- iv Sample a $\phi_k(\cdot)$ and μ_k from $p(\phi(\cdot)|B_k, X)$ and $p(\mu|B_k, X)$, respectively.

Using standard Gibbs sampling arguments, the samples of $\phi(\cdot)$ and μ drawn in the step (iv) converge to the desired posterior. As the method is based on block Gibbs sampling (Ishwaran and James, 2001), we term it *Gibbs-Hawkes*.

3.1 Conditional Distribution and Sampling of the Branching Structure

The probability of the branching structure is the product of the probabilities of the triggering relationships between pairs of points. Given μ and $\phi(\cdot)$, the probability of point t_i being triggered by point t_j is the ratio between $\phi(t_i - t_j)$ and $\lambda(t_i)$ (see e.g. (Halpin and De Boeck, 2013)),

$$\begin{aligned} p(t_i \rightarrow t_j | t_i \rightarrow \mu \vee \exists t_k < t_i : t_i \rightarrow t_k) \\ = \frac{p(t_i \rightarrow t_j)}{p(t_i \rightarrow \mu \vee \exists t_k < t_i : t_i \rightarrow t_k)} \\ = \frac{\lim_{h \rightarrow 0} \frac{p[N_{t_j}(t_i + h) - N_{t_j}(t_i) = 1]}{h}}{\lim_{h \rightarrow 0} \frac{p[N(t_i + h) - N(t_i) = 1 | H_{t_i}]}{h}} \\ = \frac{\phi(t_i - t_j)}{\mu + \sum_{t_k < t_i} \phi(t_i - t_k)}, \end{aligned} \quad (10)$$

where $t_i \rightarrow t_j$ represents t_i being triggered by t_j , N_{t_j} is the number of offspring of t_j and $H_{t_i} \equiv \{t_j : t_j < t_i\}$.

The first line of Eq. (10) is the probabilistic statement of our question and the second line is due to Bayes' rule. The third line considers an infinitesimal interval $(t_i, t_i + h)$, and takes the limit so that the ratio of probabilities is transformed as a ratio of intensities. Finally, we use the definition of the intensity. The probability of the point t_i being triggered from the background intensity is similarly computer as the ratio between μ and $\lambda(t_i)$,

$$\begin{aligned} p(t_i \rightarrow \mu | t_i \rightarrow \mu \vee \exists t_k < t_i : t_i \rightarrow t_k) \\ = \frac{\mu}{\mu + \sum_{t_k < t_i} \phi(t_i - t_k)}. \end{aligned} \quad (11)$$

Let us simplify the notation to

$$\begin{aligned} p_{i0} &\equiv p(t_i \rightarrow \mu | t_i \rightarrow \mu \vee \exists t_k < t_i : t_i \rightarrow t_k) \\ p_{ij} &\equiv p(t_i \rightarrow t_j | t_i \rightarrow \mu \vee \exists t_k < t_i : t_i \rightarrow t_k), \quad j \geq 1. \end{aligned}$$

Given these probabilities we may sample a branching structure by sampling a parent for each t_i according to probabilities $\{p_{ij}\}_{j \geq 0}$. The sampled branching structure separates a set of points into immigrants and offspring (introduced in Section 1). Immigrants can be regarded as a sequence generated from $\text{PP}(\mu)$ over Ω , where $\text{PP}(\cdot)$ is a Poisson process which has an intensity μ , and used to estimate the posterior μ .

The key property which we exploit in the subsequent Section 3.2 and Section 3.3 is the following. Denote by $\{t_k^{(i)}\}_{k=1}^{N_{t_i}}$ the N_{t_i} offspring generated by point t_i . If such a sequence is *aligned* to an origin at t_i , yielding $S_{t_i} \equiv \{t_k^{(i)} - t_i\}_{k=1}^{N_{t_i}}$, then the aligned sequence is drawn from $\text{PP}(\phi(\cdot))$ over $[0, T - t_i]$ where $[0, T]$ is the sample domain of the Hawkes process (Halpin and De Boeck, 2013). The posterior distribution of $\phi(\cdot)$ is estimated on all such aligned sequences.

3.2 Posterior Distribution of μ

Continuing from the observations in Section 3.1, note that if we are given a set of points $\{t_i\}_{i=1}^N$ generated by $\text{PP}(\mu)$ over $\Omega = [0, T]$, the likelihood for $\{t_i\}_{i=1}^N$ is the Poisson likelihood,

$$p(\{t_i\}_{i=1}^N | \mu, \Omega) = e^{-\mu T} \frac{(\mu T)^N}{N!}. \quad (12)$$

For simplicity we place a conjugate (Gamma) prior on μT (shown as Eq. (13)); the Gamma-Poisson conjugate family conveniently gives the posterior distribution of μT , *i.e.*

$$\mu T \sim \text{Gamma}(\alpha, \beta), \quad (13)$$

$$p(\mu T | \{t_i\}_{i=1}^N, \alpha, \beta) = \text{Gamma}(\alpha + N, \beta + 1). \quad (14)$$

We choose the scale α and the rate β in the Gamma prior by making the mean of the Gamma posterior

equal to N and the variance $N/2$, which is easily shown to correspond to $\alpha = N$ and $\beta = 1$. Finally due to conjugacy we obtain the posterior distribution,

$$p(\mu | \{t_i\}_{i=1}^N, \alpha, \beta) = \text{Gamma}(2N, 2T). \quad (15)$$

3.3 Posterior Distribution of $\phi(\cdot)$

We handle the posterior distribution of the triggering kernel $\phi(\cdot)$ given the branching structure in an analogous manner to the LBPP method of Walder and Bishop (2017). That is, we assume that $\phi(\cdot) = \frac{1}{2}f^2(\cdot)$ where $f(\cdot)$ is Gaussian process distributed as described in Section 2.2. In line with (Walder and Bishop, 2017), the specific kernel function we employ is the so-called *cosine kernel*,

$$k(x, y) = \sum_{\gamma \geq 0} \lambda_\gamma e_\gamma(x) e_\gamma(y) \quad (16)$$

$$\lambda_\gamma \equiv 1/(a(\sum_{j=1}^d \gamma_j^2)^m + b) \quad (17)$$

$$e_\beta(x) \equiv (2/\pi)^{d/2} \prod_{j=1}^d \sqrt{1/2}^{[\gamma_j=0]} \cos(\gamma_j x). \quad (18)$$

Here, γ is a multi-index with non-negative (integral) values, $[\cdot]$ is the indicator function, a and b are parameters controlling the prior smoothness, we have d dimensions of data, and we let $m = 2$. This basis is orthonormal over $\Omega = [0, \pi]$ with Lebesgue measure. The expansion Eq. (16) is an explicit kernel construction based on the Mercer expansion as per Eq. (3), but other kernels may be used, for example by Nyström approximation (Flaxman et al., 2017) to the Mercer decomposition.

As mentioned at the end of Section 3.1, by conditioning on the branching structure we may estimate $\phi(\cdot)$ by considering the *aligned* sequences. In particular, letting S_{t_i} denote the aligned sequence generated by t_i , the joint distribution of ω and $\{S_{t_i}\}_i$ is calculated as (Walder and Bishop, 2017)

$$\begin{aligned} &\log p(\omega, \{S_{t_i}\}_i | \Omega, k) \\ &= \log p(\{S_{t_i}\}_i | \omega, \Omega, k) + \log p(\omega) \\ &= \sum_i \left\{ \sum_{\Delta t \in S_{t_i}} \log \frac{1}{2} [\omega^T \nu(\Delta t)]^2 - \frac{1}{2} \int_{\Omega} [\omega^T \nu(t - t_i)]^2 dt \right\} \\ &\quad - \frac{1}{2} \log [(2\pi)^K |\Lambda|] - \frac{1}{2} \omega^T \Lambda^{-1} \omega. \end{aligned} \quad (19)$$

Note that there is a subtle but important difference between the integral term above and that of Walder and Bishop (2017), namely the limit of integration; closed-form expressions for the present case are provided in Appendix A.1. Putting the above equation into Eq. (6) and Eq. (7), and we obtain the mean $\hat{\omega}$ and the covariance Q of the (Laplace) approximate log-posterior in

ω . Then, according to Eqs. (8) and (9), the posterior ϕ is achieved:

$$\begin{aligned}\hat{\omega} &= \underset{\omega}{\operatorname{argmax}} \log p(\omega | \{S_{t_i}\}_i, \Omega, k) \\ &= \underset{\omega}{\operatorname{argmax}} \log p(\{S_{t_i}\}_i, \omega | \Omega, k) \\ &= \underset{\omega}{\operatorname{argmax}} \sum_i \left\{ \sum_{\Delta t \in S_{t_i}} \log \frac{1}{2} [\omega^T \nu(\Delta t)]^2 \right. \\ &\quad \left. - \frac{1}{2} \int_{\Omega} [\omega^T \nu(t - t_i)]^2 dt \right\} - \frac{1}{2} \omega^T \Lambda^{-1} \omega, \quad (20)\end{aligned}$$

where

$$\begin{aligned}Q^{-1} &= - \frac{\partial^2}{\partial \omega \partial \omega^T} \log p(\omega | \{S_{t_i}\}_i, \Omega, k) \Big|_{\omega=\hat{\omega}} \\ &= - \frac{\partial^2}{\partial \omega \partial \omega^T} \log p(\{S_{t_i}\}_i, \omega | \Omega, k) \Big|_{\omega=\hat{\omega}} \\ &= - \sum_i \left\{ \sum_{\Delta t \in S_{t_i}} \frac{2\nu(\Delta t)\nu(\Delta t)^T}{[\hat{\omega}^T \nu(\Delta t)]^2} \right. \\ &\quad \left. - \int_{\Omega} \nu(t - t_i)\nu(t - t_i)^T dt \right\} + \Lambda^{-1}. \quad (21)\end{aligned}$$

3.4 Computational Complexity

The time complexity of evaluating the LBPP objective function is $O(n^3)$ due to the inversion of an $n \times n$ matrix in Eq. (7) where n is the number of points. Interestingly, in comparison with LBPP, while our model is in some sense more complex, it enjoys a more favorable computational complexity. For our method, estimating μ given the branching structure B takes constant time. For $\phi|B$, the time complexity is $O(\sum_{i=1}^N \bar{n}_i^3)$ with $\sum_{i=1}^N n_i = N$, where n_i is the number of t_i 's offspring and \bar{n}_i^3 is the expected n_i^3 . Since the branching factor for ϕ is finite, $O(\bar{n}_i^3)$ is bounded. As a result, the time complexity for fitting $\phi|B$ is $O(N)$, that is linear in the number of points. While the naive complexity for p_{ij} is $O(N^2)$, Halpin (2012) provides methods to reducing it to $O(N)$. In summary, we have the following complexities:

Operation	Complexity
μB	$O(1)$
p_{ij}	$O(N)$
ϕB	$O(\sum_{i=1}^N \bar{n}_i^3)$ where $\sum_{i=1}^N n_i = N$

4 M.A.P Estimation

In this section, we explore the connection between our method and the EM algorithm, and we explain a simple variant which approximates EM.

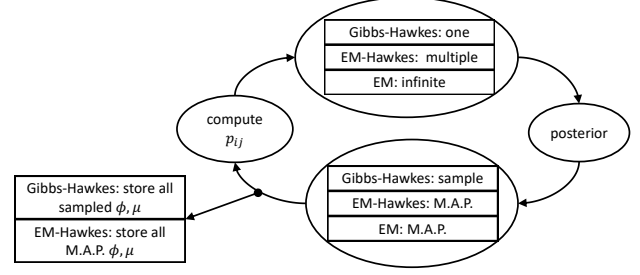


Figure 3: A visual summary of the Gibbs-Hawkes, EM-Hawkes and the EM algorithms. The differences are (1) the number of sampled branching structures and (2) selected ϕ and μ for p_{ij} . In contrast with Gibbs-Hawkes, the EM-Hawkes method draws multiple branching structures once and calculates p_{ij} with the M.A.P. ϕ and μ . The EM algorithm is equivalent to sampling infinite branching structures and exploiting M.A.P. or constrained M.L.E. ϕ and μ to calculate p_{ij} (see Section 4).

Relationship to the EM Algorithm In Section 1 we mentioned that our method is close to the stochastic EM algorithm (Celeux and Diebolt, 1985). The difference is in the M-step; to obtain an EM algorithm (Dempster et al., 1977) we need only make the following modifications; (1) sample infinite branching structures at each iteration and (2) re-calculate the probability of the branching structure with the maximum-a-posterior (M.A.P.) μ and $\phi(\cdot)$ given that infinite set of branching structures, our method would be the EM algorithm. More specifically, maximizing the expected log posterior distribution to estimate M.A.P. μ and $\phi(\cdot)$ given infinite branching structures is equivalent to maximizing the EM objective in the M-step, i.e., maximizing the constrained expected log-likelihood:

$$\begin{aligned}& \underset{\omega, \mu}{\operatorname{argmax}} \mathbb{E}_B [\log p(\omega, \mu | B, \{t_i\}_{i=1}^N, \Omega, k)] \\&= \underset{\omega, \mu}{\operatorname{argmax}} \underbrace{\mathbb{E}_B [\log p(\{t_i\}_{i=1}^N | \omega, \mu, B, \Omega, k)]}_{\text{Expected Log-likelihood}} \\&\quad + \underbrace{\log p(\omega) + \log p(\mu)}_{\text{Constraints}} \\&= \underset{\omega, \mu}{\operatorname{argmax}} \sum_{i=1}^N \left\{ \sum_{t_j < t_i} p_{ij} \log \frac{1}{2} [\omega^T \nu(t_i - t_j)]^2 - p_{i0} \log \mu \right. \\&\quad \left. - \frac{1}{2} \int_{\Omega} [\omega^T \nu(t - t_i)]^2 dt \right\} - (\beta + 1) \mu T \\&\quad - \frac{1}{2} \omega^T \Lambda^{-1} \omega - (\alpha - 1) \log \mu, \quad (22)\end{aligned}$$

where B represents the branching structure, p_{ij} the probabilities of triggering relationships shown as Eq. (10) and Eq. (11), and α, β are parameters of the Gamma prior of μT . The second line is obtained us-

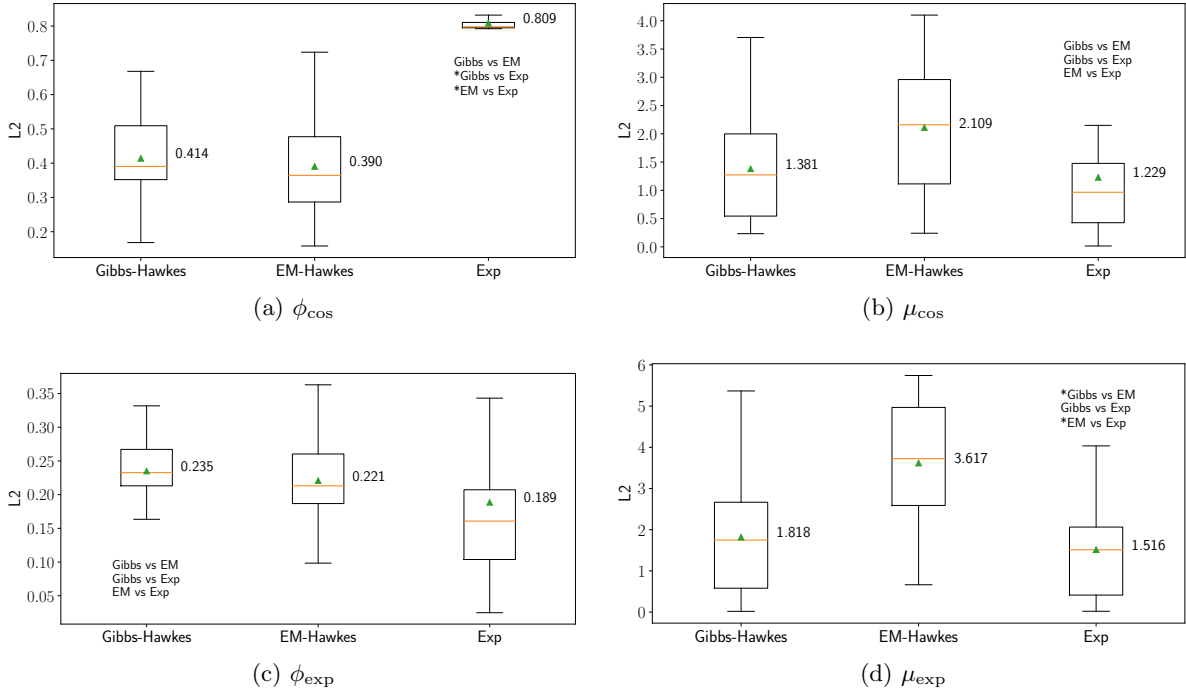


Figure 4: L2 Distance between Predicted and True $\phi(\cdot)$ and μ for Gibbs-Hawkes, EM-Hawkes and the parametric Hawkes process. Two plots on the first row are L-2 distance measured on data generated by the toy Hawkes process equipped with the cosine triggering kernel and the second row the exp triggering kernel. Each column has the median (the orange line) and the mean (number near the box and the green triangle). * before paired methods represents the statistical significance (threshold: 0.05).

ing Bayes’ rule and the third line is common in EM algorithm based estimations (Lewis and Mohler, 2011; Zhou et al., 2013). Finally, note that (2) mentioned in the beginning of this section is the same as the E-step of the EM algorithm.

EM-Hawkes The above discussion is suggestive of a variant of the Gibbs-Hawkes algorithm of Section 3, which we name *EM-Hawkes*, an approximate EM algorithm. Specifically, the difference to Gibbs-Hawkes is that EM-Hawkes (1) samples some finite number of cluster assignments (to approximate the expected log posterior distribution), and (2) finds M.A.P triggering kernels and background intensities rather than sampling them as per block Gibbs sampling (the M-step of the EM algorithm). An overview of the Gibbs-Hawkes, EM-Hawkes and EM algorithms is illustrated in Fig. 3.

Note that under our LBPP-like posterior, finding the most likely triggering kernel $\phi(\cdot)$ is intractable (shown in Appendix A.3). As an approximation we take the element-wise mode of the *marginals* of $\phi(t_i)$ to approximate the mode of posterior, $\phi(t_i)$. A natural alternative, which we found to be similar in practice, would be to take the most likely $f(\cdot)$ (which is tractable as it is multivariate Gaussian) and apply $\phi(\cdot) = \frac{1}{2}f^2(\cdot)$.

5 Experiments

In this section, we compare our proposed approaches Gibbs-Hawkes and EM-Hawkes to the parametric Hawkes, on synthetic data and on online diffusions data.

5.1 Synthetic Data

We employ two toy Hawkes processes to generate data, both having the same background intensity $\mu=10$, and cosine (Eq. (23)) and exponential (Eq. (24)) triggering kernels respectively:

$$\phi_{\cos}(t) = \begin{cases} \cos(3\pi t) + 1, & t \in [0, 1] \\ 0, & t > 1 \end{cases} \quad (23)$$

$$\phi_{\exp}(t) = 5 \exp(-5t), \quad t > 0. \quad (24)$$

Prediction For the parametric Hawkes and EM-Hawkes, the predictions μ_{pred} and $\phi_{\text{pred}}(\cdot)$ are taken to be the MAP values, while for Gibbs-Hawkes we use the posterior mean.

Evaluation Each toy model generates 400 point sequences over $\Omega = [0, \pi]$, which are evenly split into

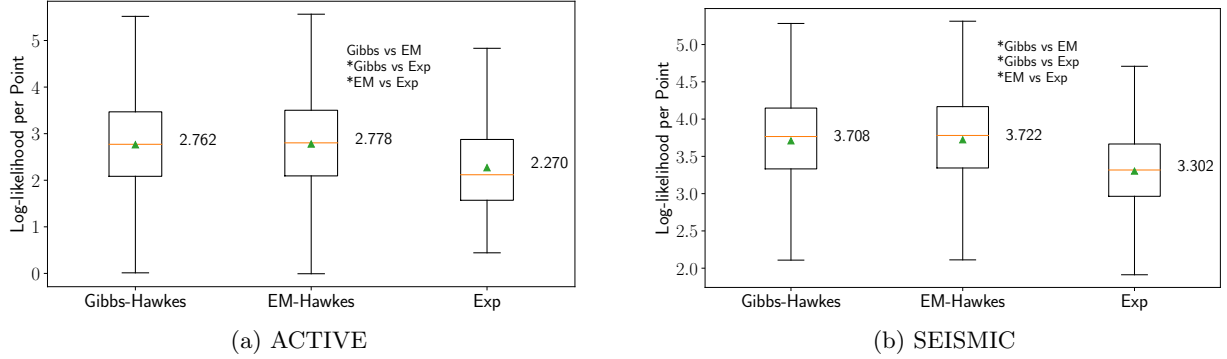


Figure 5: Holdout Log-likelihoods on Twitter diffusion data for Gibbs-Hawkes, EM-Hawkes and the parametric Hawkes process. Each box shows the mean (number near the box and [the green triangle](#)) and the median ([the orange line](#)). * before paired methods represents the statistical significance (threshold: 0.05).

40 groups, 20 for training and 20 for test. Each of the three methods fit on each group, *i.e.*, summing log-likelihoods for 10 sequences (for the parametric Hawkes) or estimating the log posterior probability of the Hawkes process given 10 sequences (for Gibbs-Hawkes and EM-Hawkes). Since the true processes are known, we evaluate based on the L2 distance between predicted and true μ and $\phi(\cdot)$,

$$d_{L2}(g_{\text{pred}}, g_{\text{true}}) = \sqrt{\int_{\Omega} [g_{\text{pred}}(t) - g_{\text{true}}(t)]^2 dt}. \quad (25)$$

Experimental details The parametric Hawkes is equipped with a constant background intensity and an exponential triggering kernel (Eq. (26), below), which has two parameters a_1, a_2 and is estimated by the maximum likelihood estimation. For Gibbs-Hawkes and EM-Hawkes, we must select parameters of the GP kernel (Eqs. (16) to (18)). Having many basis functions leads to a high fitting accuracy, but low speed. We found that using 32 basis functions provides a suitable balance. For kernel parameters a, b of Eq. (17), we choose $a, b = 0.002$. 5000 iterations are run to fit each group and first 1000 are ignored (*i.e. burned-in*).

$$\phi(t) = a_1 a_2 \exp(-a_2 t), \quad a_1, a_2 > 0. \quad (26)$$

Flexibility Fig. 4 shows the L2 distance between the learned and the true $\phi(\cdot)$ and μ on test data (for a paired t-test see the appendix Table 1). We observe that when the synthetic dataset is generated using a cosine decaying kernel (Fig. 4(a)) both Gibbs-Hawkes and EM-Hawkes perform statistically significant better than the exponential parametric form. For synthetic data generated using an exponential kernel (Fig. 4(c)), the exponential parametric version is only slightly better than our two non-parametric approaches. For estimating μ , Gibbs-Hawkes performs

similarly to the parametric method, and both methods outperform EM-Hawkes (shown in Fig. 4(b)(d)). The learned triggering kernels for ϕ_{cos} and ϕ_{exp} are shown in Figs. 2 and 6(a). In summary, our methods achieve very good performances for data generated by kernels from several parametric classes, whereas the parametric models are only efficient for data issued from their own class.

Scalability For Gibbs-Hawkes and EM-Hawkes, we record the average time taken in each iteration for different dataset sizes, shown in the appendix (Fig. 7). The ratio between the computational time and the number of points is roughly constant, which empirically confirms that the complexity of our method is $O(N)$. The main contribution to the scalability of our approaches is the stochastic branching structure which decomposes a Hawkes process into a cluster of Poisson processes. This important advantage of scalability makes our methods applicable to large datasets.

5.2 Twitter Diffusion Data

We evaluate the performance of our two proposed approaches (Gibbs-Hawkes and EM-Hawkes) on two Twitter datasets, containing retweet cascades. A retweet cascade contains an original tweet, together with its direct and indirect retweets. Current state of the art diffusion modeling approaches (Zhao et al., 2015; Mishra et al., 2016; Rizoiu et al., 2018) are based on the self-exciting assumption: users get in contact with online content, and then diffuse it to their friends, therefore generating a cascading effect. The two datasets we use in this work have been employed in prior work and they are publicly available:

- ACTIVE (Rizoiu et al., 2018) contains 41k retweet cascades, each containing at least 20

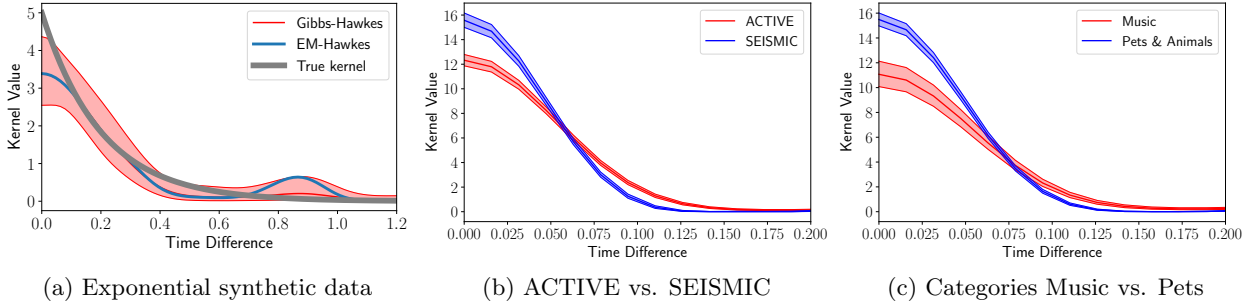


Figure 6: Learned Hawkes triggering kernels using our non-parametric Bayesian approaches. Each red or blue areas show the estimated posterior distributions for ϕ , and the solid lines indicate the 10%, 50% and 90% percentiles. (a) A synthetic dataset is simulated using $\phi_{\text{exp}}(t)$ (Eq. (24), shown in gray), and we fit it using Gibbs-Hawkes (in red) and EM-Hawkes (in blue); (b) The learned triggering kernel for Twitter cascades in ACTIVE (in red) and SEISMIC (in blue); (c) The learned triggering kernel for Twitter cascades associated with two categories in the ACTIVE set: Music (in red) and Pets & Animals (in blue)

(re)tweets with links to Youtube videos. It was collected in 2014 and each Youtube video (and therefore each cascade) is associated with a Youtube category, such as *Music*, *News* or *Film*.

- SEISMIC (Zhao et al., 2015) contains 166k randomly sampled retweet cascades, collected in from October 7 to November 7, 2011. Each cascade contains at least 50 tweets.

Setup The temporal extent of each cascade is scaled to $[0, \pi]$, and assigned to either training or test data with equal probability. We bundle together groups of 30 cascades of similar size, and we estimate one Hawkes process for each bundle. Unlike for the synthetic dataset, for the retweet cascades dataset there is no *true* Hawkes process to evaluate against. Instead, we measure using log-likelihood how well the learned model generalizes to the test set. We use the same hyper-parameters values as for the synthetic data.

Results For each dataset, we show in Fig. 5 the log-likelihood per event obtained by our approaches and by the exponential parametric Hawkes (Eq. (26)), together with significance results (detailed in the appendix Table 2). Visibly, Gibbs-Hawkes and EM-Hawkes consistently outperform the parametric method on both datasets (by 22% and 12% respectively), with EM-Hawkes obtaining slightly better performances than Gibbs-Hawkes (by 0.6% and 0.4% respectively). This seems to indicate that online diffusion is influenced by factors not captured by the parametric kernel, therefore justifying the need to learn the Hawkes kernels non-parametrically.

Interpretation We show in Fig. 6 the learned kernels for information diffusions. We notice that the

learned kernels appear to be decaying and long-tailed, in accordance with the prior literature. Fig. 6(b) shows that the kernel learned on SEISMIC is decaying faster than the kernel learned on ACTIVE. This indicates that non-specific (i.e. random) cascades have a faster decay than video-related cascades, presumably due to the fact that Youtube videos stay longer in the human attention. This connection between the type of content and the speed of the decay seems further confirmed in Fig. 6(c), where we show the learned kernels for two categories in ACTIVE: *Music* and *Pets & Animals*. Cascades relating to *Pets & Animals* have a faster decaying kernel than *Music*, most likely because *Music* is an ever-green content.

6 Conclusions

In this paper, we develop a general framework to perform non-parametric Bayesian estimations for the Hawkes processes. Our method iterates two steps. First, it samples the branching structure which transforms the Hawkes process estimations into a cluster of Poisson processes. Next, it estimates the intensity of the Hawkes process using a non-parametric Bayesian estimation of the intensity of the resulted Poisson processes. We analyze the connection between our method and the EM algorithm, and we demonstrate the flexibility and the scalability of our method on synthetic data. On two large Twitter diffusion datasets, our method outperforms the parametric Hawkes process and the learned non-parametric kernel reflects the longevity of different types of content.

Limitations and future work Our current framework is limited to the univariate unmarked Hawkes process. Future work includes extensions to the marked multivariate Hawkes process.

References

Adams, R. P., Murray, I., and MacKay, D. J. (2009). Tractable nonparametric bayesian inference in poisson processes with gaussian process intensities. In *Proceedings of the 26th Annual International Conference on Machine Learning*, pages 9–16. ACM.

Bacry, E., Dayri, K., and Muzy, J.-F. (2012). Nonparametric kernel estimation for symmetric hawkes processes. application to high frequency financial data. *The European Physical Journal B*, 85(5):157.

Bacry, E. and Muzy, J.-F. (2014). Second order statistics characterization of hawkes processes and non-parametric estimation. *arXiv preprint arXiv:1401.0903*.

Blundell, C., Beck, J., and Heller, K. A. (2012). Modelling reciprocating relationships with hawkes processes. In *Advances in Neural Information Processing Systems*, pages 2600–2608.

Celeux, G. and Diebolt, J. (1985). The sem algorithm: A probabilistic teacher algorithm derived from the EM algorithm for the mixture problem. *Computational Statistics Quarterly*, 2:73–82.

Dempster, A. P., Laird, N. M., and Rubin, D. B. (1977). Maximum likelihood from incomplete data via the em algorithm. *JOURNAL OF THE ROYAL STATISTICAL SOCIETY, SERIES B*, 39(1):1–38.

Diggle, P. J., Moraga, P., Rowlingson, B., Taylor, B. M., et al. (2013). Spatial and spatio-temporal log-gaussian cox processes: extending the geostatistical paradigm. *Statistical Science*, 28(4):542–563.

Eichler, M., Dahlhaus, R., and Dueck, J. (2017). Graphical modeling for multivariate hawkes processes with nonparametric link functions. *Journal of Time Series Analysis*, 38(2):225–242.

Flaxman, S., Teh, Y. W., and Sejdinovic, D. (2017). Poisson intensity estimation with reproducing kernels. In *Artificial Intelligence and Statistics*, pages 270–279.

Gugushvili, S., van der Meulen, F., Schauer, M., and Spreij, P. (2018). Fast and scalable non-parametric bayesian inference for poisson point processes. *arXiv preprint arXiv:1804.03616*.

Halpin, P. F. (2012). An em algorithm for hawkes process. *Psychometrika*, 2.

Halpin, P. F. and De Boeck, P. (2013). Modelling dyadic interaction with hawkes processes. *Psychometrika*, 78(4):793–814.

Hawkes, A. G. (1971). Spectra of some self-exciting and mutually exciting point processes. *Biometrika*, 58(1):83–90.

Hawkes, A. G. and Oakes, D. (1974). A cluster process representation of a self-exciting process. *Journal of Applied Probability*, 11(3):493–503.

Illian, J. B., Sørbye, S. H., and Rue, H. (2012). A toolbox for fitting complex spatial point process models using integrated nested laplace approximation (inla). *The Annals of Applied Statistics*, pages 1499–1530.

Ishwaran, H. and James, L. F. (2001). Gibbs sampling methods for stick-breaking priors. *Journal of the American Statistical Association*, 96(453):161–173.

Kirchner, M. (2017). An estimation procedure for the hawkes process. *Quantitative Finance*, 17(4):571–595.

Kurashima, T., Althoff, T., and Leskovec, J. (2018). Modeling interdependent and periodic real-world action sequences. In *Proceedings of the 27th International Conference on World Wide Web*, volume 2018, page 803. NIH Public Access.

Lewis, E. and Mohler, G. (2011). A nonparametric em algorithm for multiscale hawkes processes. *Journal of Nonparametric Statistics*, 1(1):1–20.

Lloyd, C., Gunter, T., Osborne, M., and Roberts, S. (2015). Variational inference for gaussian process modulated poisson processes. In *International Conference on Machine Learning*, pages 1814–1822.

Lloyd, C., Gunter, T., Osborne, M., Roberts, S., and Nickson, T. (2016). Latent point process allocation. In Gretton, A. and Robert, C. C., editors, *Proceedings of the 19th International Conference on Artificial Intelligence and Statistics*, volume 51 of *Proceedings of Machine Learning Research*, pages 389–397, Cadiz, Spain. PMLR.

Mercer, J. (1909). Functions of positive and negative type, and their connection with the theory of integral equations. *Philosophical Transactions of the Royal Society of London. Series A, Containing Papers of a Mathematical or Physical Character*, 209:415–446.

Mishra, S., Rizoiu, M.-A., and Xie, L. (2016). Feature Driven and Point Process Approaches for Popularity Prediction. *Proceedings of International Conference on Information and Knowledge Management - CIKM '16*. arXiv:1608.04862v2. doi:10.1145/2983323.2983812. isbn: 9781450340731.

Møller, J., Syversveen, A. R., and Waagepetersen, R. P. (1998). Log gaussian cox processes. *Scandinavian journal of statistics*, 25(3):451–482.

Rasmussen, C. E. and Williams, C. K. I. (2005). *Gaussian Processes for Machine Learning (Adaptive Computation and Machine Learning)*. The MIT Press.

Rasmussen, J. G. (2013). Bayesian inference for hawkes processes. *Methodology and Computing in Applied Probability*, 15(3):623–642.

Rathbun, S. L. and Cressie, N. (1994). Asymptotic properties of estimators for the parameters of spatial inhomogeneous poisson point processes. *Advances in Applied Probability*, 26(1):122–154.

Rizoiu, M.-A., Mishra, S., Kong, Q., Carman, M., and Xie, L. (2018). Sir-hawkes: Linking epidemic models and hawkes processes to model diffusions in finite populations. In *Proceedings of the 27th International Conference on World Wide Web*, pages 419–428. International World Wide Web Conferences Steering Committee.

Rousseau, J., Donnet, S., and Rivoirard, V. (2018). Nonparametric bayesian estimation of multivariate hawkes processes. *arXiv preprint arXiv:1802.05975*.

Rubin, I. (1972). Regular point processes and their detection. *IEEE Transactions on Information Theory*, 18(5):547–557.

Samo, Y.-L. K. and Roberts, S. (2015). Scalable nonparametric bayesian inference on point processes with gaussian processes. In *International Conference on Machine Learning*, pages 2227–2236.

Shirai, T. and Takahashi, Y. (2003). Random point fields associated with certain fredholm determinants ii: Fermion shifts and their ergodic and gibbs properties. *The Annals of Probability*, 31(3):1533–1564.

Tabibian, B., Valera, I., Farajtabar, M., Song, L., Schölkopf, B., and Gomez-Rodriguez, M. (2017). Distilling information reliability and source trustworthiness from digital traces. In *Proceedings of the 26th International Conference on World Wide Web*, pages 847–855. International World Wide Web Conferences Steering Committee.

Walder, C. J. and Bishop, A. N. (2017). Fast Bayesian intensity estimation for the permanental process. In Precup, D. and Teh, Y. W., editors, *Proceedings of the 34th International Conference on Machine Learning*, volume 70 of *Proceedings of Machine Learning Research*, pages 3579–3588, International Convention Centre, Sydney, Australia. PMLR.

Zhao, Q., Erdogdu, M. A., He, H. Y., Rajaraman, A., and Leskovec, J. (2015). Seismic: A self-exciting point process model for predicting tweet popularity. In *Proceedings of the 21th ACM SIGKDD International Conference on Knowledge Discovery and Data Mining*, pages 1513–1522. ACM.

Zhou, K., Zha, H., and Song, L. (2013). Learning social infectivity in sparse low-rank networks using multi-dimensional hawkes processes. In *Artificial Intelligence and Statistics*, pages 641–649.

A Appendix

Accompanying the submission *Efficient Non-parametric Bayesian Hawkes Processes*.

A.1 Computing the Integral Term of the Log-likelihood

We consider $\Omega = [0, T]$, the background intensity μ , $\phi(\cdot) = 1/2f(\cdot)^2$, $f(\cdot)$ defined in Eq. (4) and data $\{t_i\}_{i=1}^N$, and the integral term in the log-likelihood is calculated as below

$$\begin{aligned}
 & \text{Integral Term} \\
 & = -\frac{1}{2} \sum_{i=1}^N \int_0^T f^2(t-t_i) dt \\
 & = -\frac{1}{2} \sum_{i=1}^N \int_0^{T-t_i} \left[\sum_{k=1}^K \omega_k e_k(t) \right]^2 dt \\
 & = -\frac{1}{2} \sum_{i=1}^N \sum_{k=1}^K \sum_{k'=1}^K \omega_k \omega_{k'} \underbrace{\int_0^{T-t_i} e_k(t) e_{k'}(t) dt}_{U_{kk'}^{(i)}} \\
 & = -\frac{1}{2} \sum_{i=1}^N \boldsymbol{\omega}^T U^{(i)} \boldsymbol{\omega}. \tag{27}
 \end{aligned}$$

In our case, Eq. (18) has $d=1$, i.e., $\phi_k(x) = (2/\pi)^{1/2} \sqrt{1/2^{[k-1=0]}} \cos[(k-1)x]$, $k=1, 2, \dots$. The matrix $U^{(i)}$ is calculated as below:

$$\begin{aligned}
 U_{1,1}^{(i)} &= \int_0^{T-t_i} \frac{1}{\pi} dt = \frac{T-t_i}{\pi} \\
 U_{k>1,1}^{(i)} &= U_{1,k>1}^{(i)} \\
 &= \frac{\sqrt{2}}{\pi} \frac{\sin[(k-1)(t_m-t_i)]}{k-1} \\
 U_{k,k(k>1)}^{(i)} &= \frac{1}{\pi} \left\{ T-t_i + \frac{\sin[2(k-1)(T-t_i)]}{2(k-1)} \right\} \\
 U_{k,k'(k \neq k')}^{(i)} &= \frac{1}{\pi} \left\{ \frac{\sin[(k-k')(T-t_i)]}{k-k'} + \right. \\
 &\quad \left. \frac{\sin[(k+k'-2)(T-t_i)]}{k+k'-2} \right\}.
 \end{aligned}$$

A.2 Paired T-test for Synthetic and Real Life Data

The threshold for statistical significance is 0.05 and paired t-test results are in Tables 1 and 2

A.3 Mode-Finding the Triggering Kernel

Here we demonstrate in detail the computational challenges involved in finding the posterior mode with respect to the value of the triggering kernel at multiple

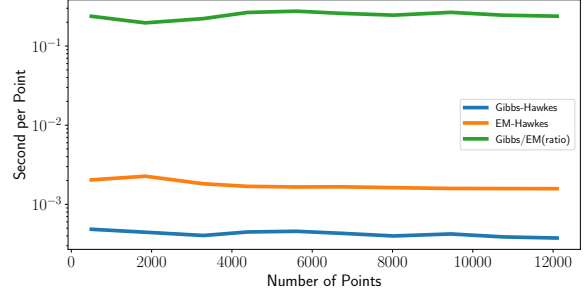


Figure 7: Fitting Time per Point in One Iteration.

Table 1: Paired T-test for Synthetic Data

Functions	Pairs	t	p
ϕ_{\cos}	Gibbs-EM	1.452	0.163
	Gibbs-exp	-12.599	1.133×10^{-10}
	EM-exp	-12.442	1.402×10^{-10}
μ_{\cos}	Gibbs-EM	-1.866	0.077
	Gibbs-exp	0.946	0.356
	EM-exp	2.049	0.055
ϕ_{\exp}	Gibbs-EM	1.714	0.103
	Gibbs-exp	1.154	0.263
	EM-exp	0.854	0.404
μ_{\exp}	Gibbs-EM	-4.227	0.0005
	Gibbs-exp	0.588	0.563
	EM-exp	3.867	0.001

Table 2: Paired T-test for Real Life Data

Data	Pairs	t	p
ACTIVE	Gibbs-EM	-1.357	0.175
	Gibbs-exp	62.320	0.0
	EM-exp	44.970	0.0
SEISMIC	Gibbs-EM	-3.090	0.002
	Gibbs-exp	98.651	0.0
	EM-exp	99.524	0.0

point locations. Consider the triggering kernel $\phi(\cdot) = \frac{1}{2}f^2(\cdot)$ where $f(\cdot)$ is Gaussian process distributed. For a dataset $\{t_i\}_{i=1}^N$, $\mathbf{X} \equiv \{f(t_i)\}_{i=1}^N = \{X_i\}_{i=1}^N$ has a normal distribution, i.e., $\{f(t_i)\}_{i=1}^N \sim \mathcal{N}(\mathbf{m}, \mathbf{\Sigma})$ where \mathbf{m} and $\mathbf{\Sigma}$ are the mean and the covariance matrix. The distribution of $\mathbf{Y} \equiv \{\phi(t_i)\}_{i=1}^N = \{Y_i\}_{i=1}^N$ is derived as below where F is the cumulative density function and

f the probabilistic density function.

$$\begin{aligned}
 & F_{\mathbf{Y}}(\mathbf{y}) \\
 &= P(-\sqrt{2y_1} < X_i < \sqrt{2y_i}, i=1, \dots, N) \\
 &= \int_{-\sqrt{2y_1}}^{\sqrt{2y_1}} \dots \int_{-\sqrt{2y_N}}^{\sqrt{2y_N}} \frac{1}{\sqrt{(2\pi)^N \Sigma^{-1}}} \\
 & \exp\left[-\frac{(\mathbf{X}-\mathbf{m})^T \Sigma^{-1} (\mathbf{X}-\mathbf{m})}{2}\right] dX_1 \dots dX_N \\
 & f_{\mathbf{Y}}(\mathbf{y}) \\
 &= \frac{\partial^N}{\partial y_1 \dots \partial y_N} F_{\mathbf{Y}}(\mathbf{y}) \\
 &= \frac{1}{\sqrt{(2\pi)^N \Sigma^{-1}}} \left(\prod_{i=1}^N \frac{1}{2\sqrt{2y_1}} \right) \\
 & \sum_{\mathbf{X} \in \times_{i=1}^N \{\sqrt{2y_1}, -\sqrt{2y_1}\}} \exp\left[-\frac{(\mathbf{X}-\mathbf{m})^T \Sigma^{-1} (\mathbf{X}-\mathbf{m})}{2}\right], \tag{28}
 \end{aligned}$$

where \times is the Cartesian product. There are 2^N summations of exponential functions, which is intractable.